Switching dynamics in vanadium dioxide-based stochastic thermal neurons

Haoming Yu[1], A.N.M. Nafiul Islam[2], Sandip Mondal[1], Abhronil Sengupta[2], Shriram Ramanathan[1]

***Abstract*— We report on switching dynamics of individual and coupled vanadium dioxide (VO_2) devices subject to voltage pulses as the temperature is systematically varied from room temperature spanning the insulator-metal transition (IMT) temperature. The switching voltage of single devices have a strong relationship with both temperature and voltage pulse width. Two-step switching in connected VO_2 devices has been noted in current transient plots and was found to depend on temperature, pulse width, and pulse amplitude. Experimental switching behavior measured from VO_2 artificial neurons were implemented into a spiking neural network (SNN). During training, modulating the switching voltage via temperature affords a novel method to implement homeostasis with the coupled devices. Simulation results show the efficacy of the stochastic neuronal characteristics and the proposed homeostasis mechanism on a standard digit recognition task. These studies contribute to on-going efforts in neuromorphic computing exploiting collective phase transitions.**

***Index Terms*— phase transition, VO_2, artificial neuron, computing**

I. INTRODUCTION

Vanadium oxide (VO_2) undergoes a first order metal-to-insulator transition (MIT), which causes a conductivity change of several orders of magnitude. This phase transition can be induced by both thermal and voltage stimuli [1, 2]. When electric field of sufficient amplitude is applied, a phase transition from insulating phase to metallic phase occurs [3]. The threshold switching behavior is interesting for designing selectors in crossbar memories arrays, neuromorphic devices such as artificial neurons [4, 5], and resistive memories [6, 7].

The MIT behaviour of VO_2 results in a current spike and can be utilized to emulate the behaviour of a biological neuron when threshold firing voltage is reached [3]. Hence, there is growing interest in studying the transient characteristic of VO_2 E-IMT under short pulses. Murtagh et al. [8] studied the effect of the time delay between consecutive voltage pulses on the hysteresis loop of VO_2 E-IMT. They showed the joule heating from previous pulses affects latter pulse dynamics and proposed modulating the E-IMT behaviour of VO_2 through pulse history. Lin et al. [9] developed an electrothermal model based on E-IMT joule heating. The output current curve was divided into three parts, the incubation period, positive feedback period and width expansion period. Patlagan et al. [10] applied millisecond time scale pulsed I-V measurements on $Al_xV_{1-x}O_2$ bulk crystals to study hysteresis and thermal effects driving switching. Tungsten doping in VO_2 has recently been shown as an effective way to control the threshold switching voltage [11]. These results demonstrate the on-going progress towards exploring the use of phase transitions in emerging electronic devices.

To further advance our understanding, it is important to understand the interaction of the E-IMT devices when they are interconnected in a circuit [12, 13]. Moreover, interaction behavior is unknown when each device is heated to a different temperature while connected in a circuit. Thus, measurements of device behaviour in simple circuits when excited with fast electric pulses could help in elucidating the behavior of VO_2 switches and the data can be used as input for simulations.

Here, we first studied the switching dynamics of individual VO_2 devices held at different temperatures. The mean switching voltage for a single out-of-plane device (300 nm VO_2 film thickness) is 2.1 V. We demonstrate the close relationship between temperature of the device and triangular pulse width to the switching voltage of a single device. We then investigate the interaction of VO_2 devices held at different temperatures while connected in a circuit. A triangular pulse of width of the order of 10 μs is applied to extract the behavior of the circuit. Two-step E-IMT is observed at room temperature with two distinct current spikes at 4 V and 4.2 V when two devices are connected in series. The two steps correspond to the individual E-IMT of each device. Input voltage to trigger the E-IMT of a device kept at 25 °C was reduced by 0.77 V when a second connected device was heated to 60 ℃. This modulation of triggering voltage can be utilized to implement homeostasis in a novel manner for SNNs. As proof-of-concept, a simulated SNN was trained on the standard MNIST digit recognition dataset [14] to showcase the efficacy of both the stochastic neurnonal characteristics and the thermal-coupling enabled homeostasis mechanism, achieving a test accuracy of 88.9%.

II. EXPERIMENTAL

A. Characterization and device fabrication

The devices were fabricated using 300 nm VO_2 thin film deposited on to highly doped n-Si substrate ($\rho = 0.001\ \Omega \times cm$) with a native oxide layer (SiO_2/n-Si). The deposition was conducted with an AJA sputter deposition system, using a V_2O_5 target at 650 °C in 99.994 % Ar/ 0.06 % O_2 gas mixture at 5 mTorr. The film thickness was measured through cross-

[1] Haoming Yu, Sandip Mondal, Shriram Ramanathan are with the School of Materials Engineering, Purdue University, West Lafayette, IN 47907 USA (e-mail: yu957@purdue.edu and shriram@purdue.edu)

[2] A. N. M. Nafiul Islam, Abhronil Sengupta are are with the School of Electrical Engineering and Computer Science, Penn state University, State College, PA 16801 USA)

sectional SEM. Circular Pd electrodes with varying diameter of 100 µm, 200 µm, 300 µm were fabricated using sputtering on VO_2 film through shadow masks. The back contact of the device was formed after removing the oxides and painting with silver paste. The device structure is shown in Fig. 1 (a).

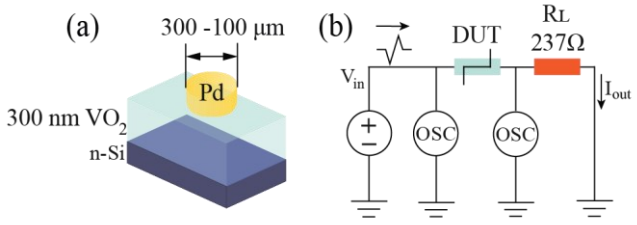

Fig. 1 (a) 300 nm VO_2 thin film was sputtered on n-Si substrate with a native oxide layer. The top electrode is sputtered Pd and the bottom electrode is formed after removing the oxide on back side of Si and painting with silver paste (b) Schematic of the high speed measurement set up.

B. Test circuit design

The test circuit is designed by connecting the device(s) under test (DUT) and a load resistor (R_L) of 237 Ω in series. Voltage pulses with a pulse width ranging from 10 µs to 1 ms were applied to the DUT with a signal generator (Tektronics AFG 31000). One channel of a oscilloscope (Keysight MSOX4154A) is connected across the whole circuit to capture the input voltage (V_{in}), while another channel is connected across the load resistor to acquire the voltage drop across it (V_R). To determine the current through the circuit (I_{out}), the equation $I_{out} = R_L/V_R$ is used. A hot stage is placed under the DUT when excitation above room temperature is needed. The experimental set up is shown in Fig. 1 (b).

C. *Data processing*

The oscilloscope has a sampling rate of 400 ps. This causes a large random noise. Voltage data collected by the oscilloscope in 40 ns (100 data points) when the voltage is held stable is used to analysis the noise of the test. The standard deviation of the signal is 0.03 V. A smoothing of the data is performed as follows: every data point is acquired by averaging the sum of 50 points before and 49 points after that specific data point. This reduces random noise collected during experiment, but avoids loss of data density.

III. RESULTS AND DISCUSSION

X-ray diffraction (XRD) pattern verified the successful growth of the VO_2 oxide layer on top of the SiO_2/n-Si substrate, as shown in Fig. 2 (a). Multiple VO_2 diffraction peaks were identified in the XRD graph, indicating the polycrystalline nature of the thin film. Detailed VO_2 peak position and peak intensity comparison with reference XRD data is included in table I. All peak intensities are normalized to the intensity of (011) peak from reference data. The reference XRD data in the table is from polycrystalline VO_2 powder diffraction. Comparing the collected XRD peak intensity and reference data [15], the peaks aside from (011) have significantly smaller relative intensities. This implies the as-grown VO_2 thin film is textured. Moreover, the XRD patterns of the thin film from 45 °C to 100 °C were collected at a heating rate of 10 °C/ hour and a hold time of 2h for the measurement. A peak shift from VO_2 M (011) to VO_2 R (110) is observed when the excitation temperature reaches 70 ºC, and the peak shifting stabilized after 75 ºC, marking the evolution of the structural transition. Zoomed-in XRD pattern of temperature dependent evolution of M (011) to R (110) peak is shown in Fig. 2(b).

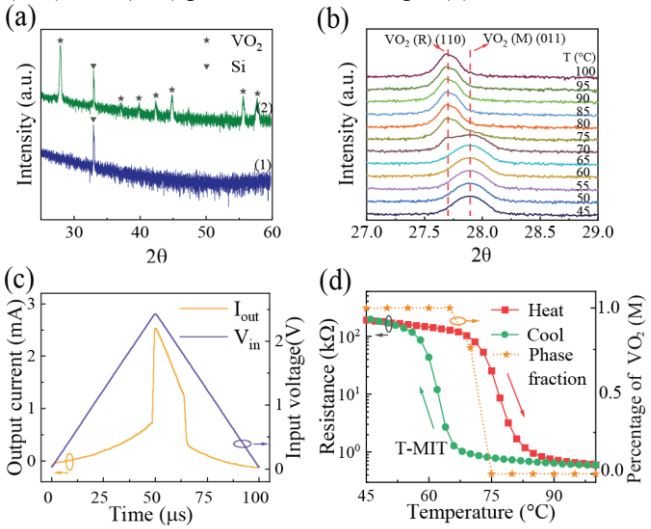

Fig. 2 (a) (1) X-ray diffraction (XRD) pattern of bare n-Si substrate (2) XRD pattern of 300 nm VO_2 grown on n-Si/SiO_2. (b) Enlarged XRD pattern of VO_2 M (011) and VO_2 R (110) peaks when temperature is changed from 45 °C to 100 °C. (c) Single VO_2 device E-IMT behavior. A triangular pulse of 100 µs, 2.5 V is applied across the VO_2 vertical device with a 237 Ω load resistor connected in series. (d) Temperature induced phase transition of VO_2 vertical devices. The red and green line shows the resistance versus temperature trend when heating/cooling the device. The orange line shows the evolution of phase fraction (from XRD) of VO_2 M phase and VO_2 R phase with temperature when heating the device.

Table I 25ºC VO_2 peak position and relative intensity

Peak	2θ (º)	Relative intensity (%)	2θ (º) (reference [15])	Relative intensity (%) (reference [15])
(011)	27.895	100	27.872	100
($\bar{2}$02)	37.131	1.8	36.889	12.0
(200)	37.461	1.8	36.999	32.4
(020)	39.823	2.4	39.724	3.8
(002)			39.798	3.2
(210)	42.345	4.4	42.271	9.1
(012)	44.776	10.0	44.667	3.1
(021)				
(211)	55.631	9.9	55.514	25.1
(022)	57.671	20.8	57.419	15.3

The characteristics of a single VO_2 device was first studied to provide a baseline dataset. Fig. 2 (c) demonstrates the E-IMT behavior of single device when a pulse of 2.5 V/ 100 µs was applied. A distinct current spike is observed when the input voltage is 2.5 V. An overlay of resistance versus temperature (R-T) and monoclinic phase fraction estimated from XRD versus temperature is shown in Fig. 2 (d). The resistance is extracted from the slope of linear IV sweep from -0.1 V to 0.1 V at various temperatures. The phase fraction data were extracted from temperature dependent change of the ratio between VO_2 M (011) and VO_2 R (110) (Fig. 2 (b)). Hysteresis can be observed in the R-T curve explaining the asymmetry of the I-t curve when a triangular pulse is applied to the VO_2

device. The temperature of the begin of structural transition is in between 65 °C to 70 °C as shown in the phase fraction data in Fig. 2 (d). Also, the phase fraction curve sits right between the R-T hysteresis loop.

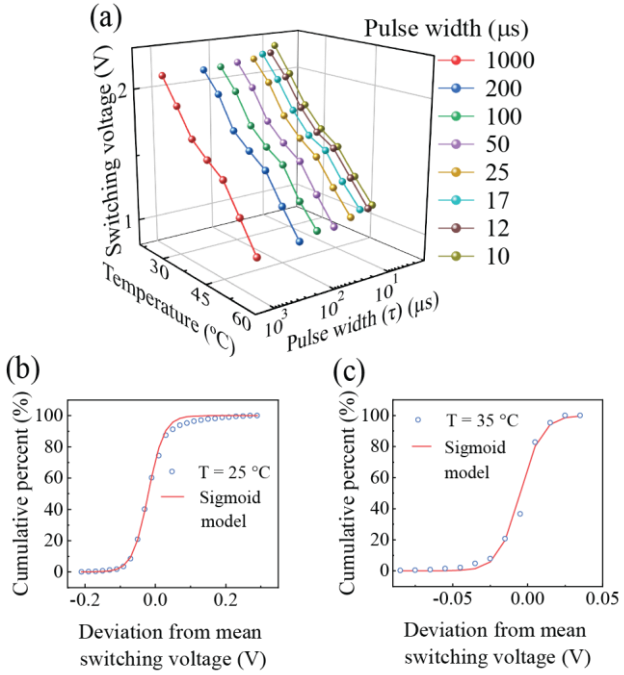

Fig. 3 (a) Relationship of switching voltage with temperature and pulse width (τ). Temperature ranges from 25 °C to 50 °C, while pulse width is varied from 10 μs to 1000 μs. (b) statistical data of deviation from mean switching voltage of device at 25 ºC (c) and 35 ºC for 1800 cycles. Raw data is shown with blue circles and the sigmoid function fitted to data is shown in red curve.

The T-IMT and E-IMT shows different current jump ratios. The T-IMT ratio is calculated with the resistance at 45 ºC and 90 ºC in Fig. 2(d), while the E-IMT ratio is calculated by the current after and before the current jump in Fig. 2 (c). Similar phenomenon has been reported and it has been shown that the load resistor in the measurement set up limits the current jump of E-IMT [16]. The difference may also be caused by the filamentary nature of the phase transition as it propagates [17]. Electron injection [18] and thermal runaway [19-21] mechanisms have also been noted in other threshold switching materials indicating a general mechanism for phase switching. The power per spike is ~ 4 nJ, calculated with the power supplied by the pulse generator (V_{in} × I_{out}) during the rising edge of E-IMT in Fig. 2 (c). The unit device area power per spike is 54 fJ/μm^2. As a comparison, for a 100 nm^2 device reported in literature, the power per spike per area is of the order of 10 pJ/μm^2 [22]. It has been shown that the power per spike of VO_2 neurons scales with device size [23], thus, shrinking the device geometry would correspondingly reduce energy per spike.

Switching voltage (V_{switch}) is mapped against the width of triangular pulse and the temperature of device (Fig. 3 (a)). Switching voltage is acquired by subtracting the voltage drop across the load resistor from the input voltage ($V_{switch} = V_{in} - V_R$). As shown in Fig. 3 (a) switching voltage is highly correlated with the temperature. The mean room temperature switching voltage tested with 1000 μs triangular pulse is 2.1 V. This would correspond to a threshold electric field of 7 × 10^6 V/m for a 300 nm thick channel. Statistical data of switching voltage for 1800 cycles were measured from a VO_2 device at 25 ºC and 35 ºC as shown in Fig. 3 (b) and (c). The room temperature (25 ºC) variation range is from -0.2 V to 0.3 V, while more than 92 % of switching voltage at room temperature falls in -0.1 V to 0.1 V deviation from mean switching votlage. This switching voltage variation has been ascribed to the randomness in domain orientation [24] and nucleation of phases [25]. The statistical data is also fitted with sigmoid function for simulation of a stochastic neuron.

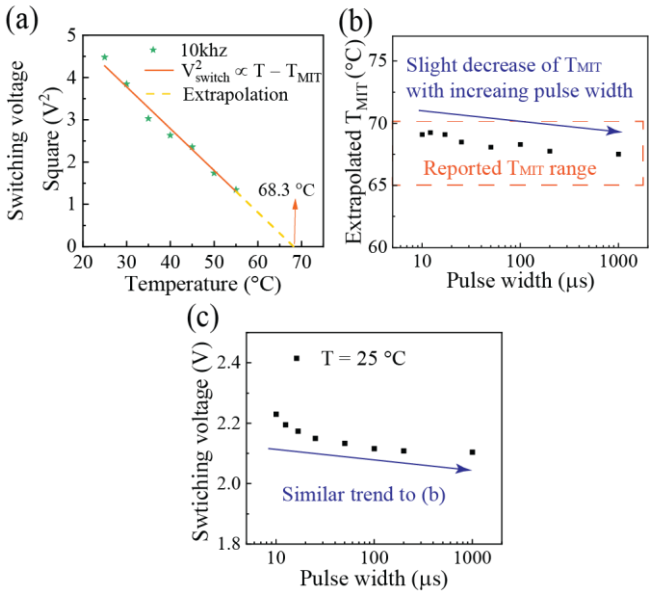

Fig. 4 (a) Linear fitting of square of switching voltage (V^2_{switch}) and temperature. The fitting curve is extrapolated and intercepts the temperature axis at 68.3 °C. (b) Extrapolated IMT temperature (T_{IMT}) from switching voltage (V^2_{switch}) and temperature of different pulse width. The fitting and extrapolation process is the same as (a). (c) A slight decrease in switching voltage with pulse width is shown.

Employing E-IMT electrothermo model from literature [26], $V^2_{switch} \propto T - T_{IMT}$, a fitting was obtained. The fitted curve shown in Fig. 4 (a) corresponds to data collected with 100 μs triangular pulses. The extrapolation of the fitted curve intercepts the temperature axis at 68.3 °C. This is a good estimate for the insulator to metal transition temperature (T_{IMT}), and falls in range of T_{IMT} reported previously [27-28]. Extrapolation of the fitting curve for data sets collected at other pulse frequencies also renders similar results (Fig. 4 (b)). We also notice that there is a slight increase in the T_{IMT} with decreasing pulse width. This is likely caused by the decrease of switching voltage with increasing pulse width across all temperatures (Fig. 4 (c) shows a representative data set).

Next, a VO_2 circuit was designed by connecting two VO_2 devices in series through a 237 Ω load resistor. The test circuit is shown in Fig. 5 (a) for reference. Hot plates were used for controlling the temperature of individual devices.

The switching behavior of the circuit where two VO_2 devices were connected is shown in Fig. 5 (b). A 4.4 V/ 10 μs duration triangular pulse was applied . Two distinct current spikes were observed at 4.29 μs and 4.76 μs. The rise time for the two spikes were 130 ns and 190 ns respectively. The VO_2 devices switched back to insulating state at 7.5 μs. Two – step switching phenomenon is also observed when the pulse width was varied from 10 μs to 1 ms corresponding to the E-IMT of each connected device. The individual behavior of each of the connected devices is shown in Fig. 5 (c-d). The two-step

switching is only seen across the connected devices. The difference in the switching voltage is likely due to the subtle heterogeneity in the as-deposited film, causing slight differences in the behavior of individual devices. The two-step switching can also be controlled through applied pulse amplitude. Fig. 5 (e) shows the I-t curve evolution with respect to triangular pulse amplitude. Only one current spike is observed when the amplitude of the pulse is 4 V. Two-step switching onsets when the pulse amplitude is 4.2 V and higher. The peak current increased with pulse amplitude (A_{pulse}) linearly when $A_{pulse} > 4.6$ V, indicating that the transition to metallic state is fully triggered in both devices (as shown in Fig. 5 (f)). This indicates the "on" resistance of D1 and D2 is not affected when triangular pulses with an amplitude larger than 4.6 V is applied.

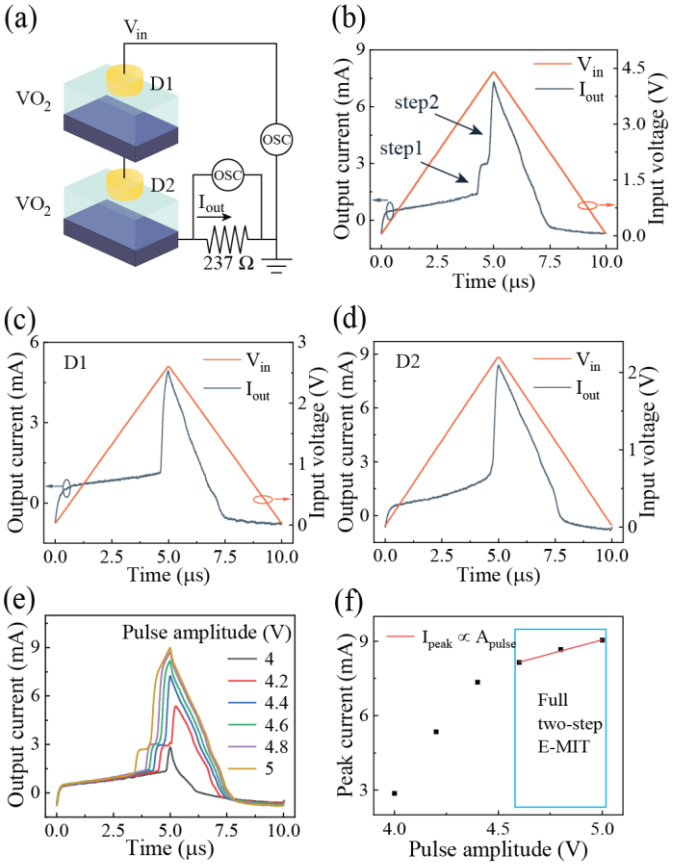

Fig. 5 (a) Test circuit with two VO_2 devices placed at room temperature and connected through a load resister of 237 Ω. (b) Pulse current is measured with two-step switching behavior with respect to triangular input pulse of amplitude 4.4 V and width 10 μ s. (c) (d) single device spiking behavior of D1 and D2 respectively. (e) Variation of two-step switching for different pulse amplitude. (f) Change in peak current (I_{peak}) for different pulse amplitude (A_{pulse}). A linear relationship of I_{peak} and A_{pulse} is observed when $A_{pulse} > 4.6$ V.

To study the interaction behavior between VO_2 devices in a circuit, one of the VO_2 devices was slowly heated while the other device was kept at 25 °C. The experimental set up is shown in Fig. 6 (a). In this case, D2 is heated and the resulting I-t curve evolution with respect to temperature is shown in Fig. 6 (b). Two step switching is clearly seen when D2 was kept at 35 °C. The input voltage to trigger its E-IMT decreases with respect to increase in temperature. No E-IMT in D2 is observed when its temperature is > 60 °C. This behavior corresponds to VO_2 undergoing a phase transition at around 68 °C. Since 60 °C is very close to the phase transition temperature, minimal

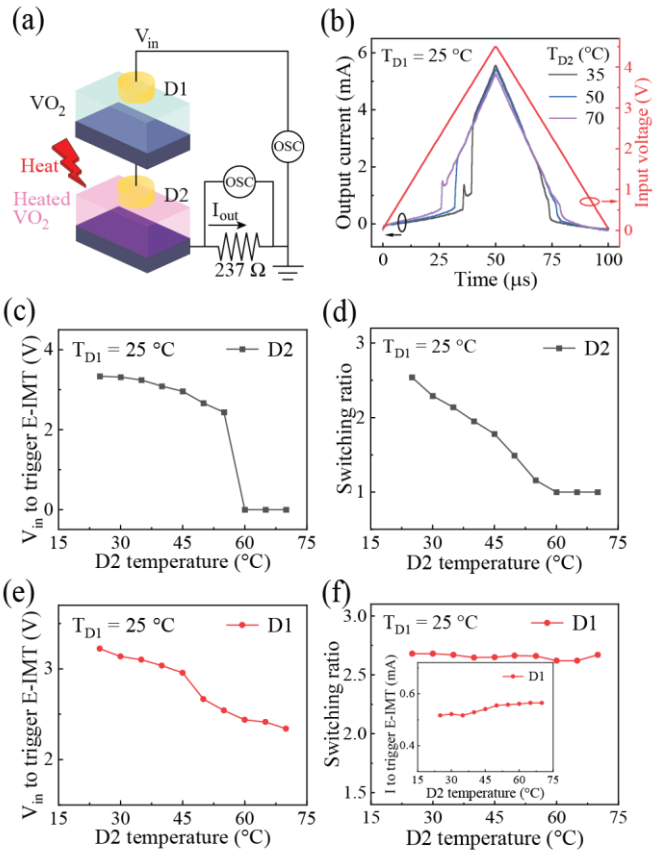

Fig. 6 (a) In the circuit, device 1 (D1) was placed at room temperature, while device 2 (D2) was heated from 25 °C to 70 °C. (b) Two-step switching behavior evolution of the connected VO_2 with respect to temperature. The input triangular pulse has a pulse width of 100 μs and an amplitude of 4.5 V. (c) Evolution of input voltage to trigger D2 E-IMT with D2 excitation temperature. (d) Evolution of switching ratio (I_{on}/I_{off}) of D2 with D2 excitation temperature. (e) Evolution of input voltage to trigger D1 E-IMT with D2 excitation temperature. (f) Evolution of switching ratio (I_{on}/I_{off}) of D1 with D2 excitation temperature. The inset shows the current to trigger E-IMT of D1 with respect to D2 temperature.

heating is sufficient to induce a phase transition. The described trend is shown in Fig. 6 (c). A decrease in switching ratio of D2 device is shown in Fig. 6 (d). The switching ratio (I_{on}/I_{off}) is calculated by the ratio between current right after and before device D1/D2 go through E-IMT. This corresponds to results of single device resistance versus temperature curve, where the resistance of VO_2 decreases with temperature in insulating state (Fig. 2 (d)). The change of D2 temperature affects the input voltage to trigger the E-IMT of D1, as shown in Fig. 6 (e). We attribute this observation to the voltage divider effect when two resistors are connected in series. When the excitation temperature of D2 is elevated, the resistance of the insulating state decreases. This increases the voltage drop across D1, leading to a decrease in the input voltage to initiate E-IMT of D1. In addition we also noticed the switching ratio of D1 is independent of excitation temperature of D2 (Fig. 6 (f)). This corresponds to the fact that switching ratio is an intrinsic characteristic of individual devices. The inset in Fig. 6 (f) shows that the current to trigger the E-IMT of D1 has only a slight increase with increasing temperature. The increase (0.05 mA) is within 10% of the current to trigger E-IMT at 25 °C (0.517 mA). If the initial resistance of D1 before E-IMT stays

the same, it is likely the power to trigger the E-IMT of D1 does not vary as D1 temperature changes. Similar measurements were performed on D2 (held at 25 °C) when D1 was kept at variable temperature (25 °C to 70 °C). This demonstrates that the input voltage to trigger D2 E-IMT is independent of the temperature of D1.

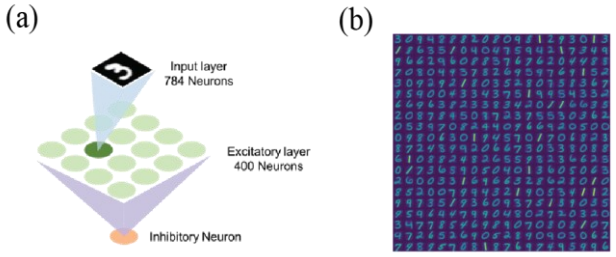

Fig. 7 (a) Spiking Neural Network simulated with the VO_2 devices as stochastic neurons. The input layer consists of 784 neurons (28 × 28), followed by 400 neurons each in the excitatory and inhibitory layer. The network architecture was adopted from Ref. [29], (b) The learnt weight patterns after training over 60,000 training images of the MNIST dataset.

The change in temperature in one VO_2 device (D2) modulating the switching behavior of another device (D1) whilst also preserving the switching ratio can be a useful behavior of connected threshold switches. Previously, the switching of the IMT devices, which is probabilistic in nature, has been shown to emulate spiking neurons [30]. The additional control mechanism afforded by the temperature modulation can be used during training for homeostasis. In homeostasis, a single neuron is prevented from dominating the spiking pattern by making it harder for neurons to spike that have already spiked [29] and is a crucial enabling feature for learning in a SNN. Since such a property is neuron-specific, implementing homeostasis in crossbar array based systems requires complex peripheral scaling circuity interfaced with each crossbar column that scales the column output (or equivalently neuron input) accordingly [31]. Approaches to reduce the scaling circuitry to a single device in series with the stochastic VO_2 neuron will be of interest in edge computing devices. In our proposed system, at the beginning of training, the control VO_2 device (D2) is heated which results in the lowest median switching voltage for our VO_2 neuron (D1). As the training progresses, the control device cools which results in the switching voltage of the neuron to increase, thus achieving homeostasis (Fig. 6 (e)).

In a neural network, neurons may be interfaced with crossbar arrays of programmable synapses. In our network, the neurons are stochastic meaning the probability of firing at any particular time is a non-linear function of the instantaneous post-synaptic input. The measured probability of the VO_2 device's switching shows a sigmoidal dependence to the input voltage (Fig. 3 (b,c)). A spiking neural network (SNN) with the VO_2 devices as neurons is simulated for the standard digit recognition problem based on the MNIST dataset [14]. We use the PyTorch-based BindsNET [32] open-source library and the network architecture is adopted from [30] and is shown in Fig. 7 (a) consisting of an input layer of 784 neurons and an excitatory and an inhibitory layer of 400 neurons each. The excitatory neurons are connected in a one-to-one manner with the inhibitory neurons, such that, a spike in the excitatory neuron triggers a spike in its corresponding inhibitory neuron. The inhibitory neruons, on the other hand, are connected back to all the excitatory neurons, except for the one it receives a connection from. When an inhibitory neuron spikes, it inhibits all the other excitatory neurons, i.e., stops them from firing. This mechanism is known as lateral inhibition and leads to competition among excitatory neurons.

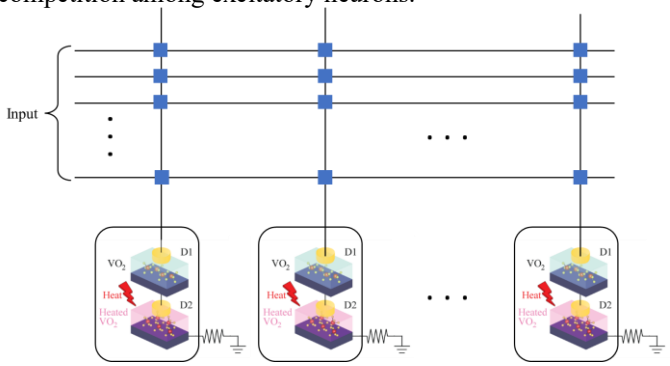

Fig. 8 Simulated implementation in a crossbar array with stochastic VO_2 neuron. At each cross-point there is a programmable synapse. Inputs get modulated by the crossbar and the neurons receive the weighted summation of the input. The neuron probabilistically switches based on the input. Thermal coupling enables homeostasis functionality.

Table II network simulation parameters

Parameter	**Value**
Post and Pre-synaptic learning rate, A_+, A_-	10^{-2}, 10^{-4}
Refractory period	5 timesteps
Time constant for STDP dynamics, τ_+, τ_-	20.0
Synaptic weights from excitatory to inhibitory layer, $w_{exc-inh}$	22.5
Synaptic weights from inhibitory to excitatory layer, $w_{inh-exc}$	240
Normalization factor	78.4

Such a network can be implemented using a crossbar array of synaptic devices (Fig. 8). The input is presented to the network for 100 timesteps as Poisson spike trains whose frequency is proportional to the input pixel intensity and summed according to Kirchhoff's law. The input is then applied across the VO_2 neuron, which generates the spikes in a probabilistic manner according to the sigmoidal function. Homeostasis is implemented by the second VO_2 device's temperature modulation (Fig. 6 (e)). The weight update happens in an unsupervised manner according to Spike-Timing Dependent Plasticity (STDP) [30, 33] as given by Eq. 1.

$$\Delta w = \begin{cases} \eta_+ \exp\left(\frac{-\Delta t}{\tau_+}\right) & for\ \Delta t > 0 \\ \eta_- \exp\left(\frac{\Delta t}{\tau_-}\right) & for\ \Delta t < 0 \end{cases} \quad \ldots\ldots\ldots\ldots\ldots (1)$$

The network simulation parameters are given in Table II. We find the network is able to successfully learn (Fig. 7 (b)) and achieves an accuracy of 88.9% over the test set after 2 epochs of training. This is comparable to accuracies reported for ideal software based networks with 400 neurons [29] and can be increased further in future by increasing the number of nodes in the network.

IV. Conclusion

We have systematically characterized the electrical switching characteristics of individual and coupled VO_2 devices as function of voltage pulse profile and temperature. In connected devices, the temperature of one device could affect the input voltage to trigger the IMT of another device. This observation could be explained by the voltage divider effect. A method for temperature-controlled homeostasis was proposed and experimentally measured stochastic switching behavior was implemented in a neural network to demonstrate digit recognition with accuracy comparable to software-based networks.

Acknowledgement

This research is supported as part of the center for 3D Ferroelectric Microelectronics (3DFeM), an Energy Frontier Research Center funded by the U.S. Department of Energy (DOE), Office of Science, Basic Energy Sciences under Award Number DE-SC0021118 (stochastic thermal neuron model) and by National Science Foundation Award No. 1904081 (synthesis and measurement of electrical properties).

References

[1] G. Seo et al., "Voltage-pulse-induced switching dynamics in VO_2 thin-film devices on silicon" *IEEE Electr. Device L.*, vol. 32, no. 11, pp. 1582-1584, Sep. 2011. doi: 10.1109/LED.2011.2163922.

[2] B.-G. Chae, H.-T. Kim, D.-H. Youn, and K.-Y. Kang , "Abrupt metal–insulator transition observed in VO_2 thin films induced by a switching voltage pulse," *Physica. B*, vol. 369, no. 1-4, pp. 76-80, Dec. 2005. doi: 10.1016/j.physb.2005.07.032.

[3] Y. Zhou and S. Ramanathan, "Mott memory and neuromorphic devices," *P. IEEE*, vol. 103, no. 8, pp. 1289-1310, Aug. 2015. doi: 10.1109/JPROC.2015.2431914.

[4] S. Lashkare, P. Kumbhare, V. Saraswat, and U. Ganguly, "Transient joule heating-based oscillator neuron for neuromorphic computing," *IEEE Electr. Device L.*, vol. 39, no. 9, pp. 1437-1440, Jul. 2018. doi: 10.1109/LED.2018.2854732.

[5] Y. Shi and L.-Q. Chen, "Current-driven insulator-to-metal transition in strongly correlated VO_2," *Phys. Rev. Applied*, vol. 11, no. 1, pp. 014059, Jan. 2019. doi: 10.1103/PhysRevApplied.11.014059.

[6] T.-H. Yeh et al., "Enhancing threshold switching characteristics and stability of vanadium oxide-based selector with vanadium electrode," *IEEE T. Electron Dev*., vol. 67, no. 11, pp. 5059-5062, Sep. 2020. doi: 10.1109/TED.2020.3019773.

[7] A. G. Shabalin et al., "Nanoscale imaging and control of volatile and non-volatile resistive switching in VO_2," *Small*, vol. 16, no. 50, pp. 2005439, Nov. 2020. doi: 10.1002/smll.202005439.

[8] O. Murtagh, B. Walls, and I. Shvets, "Controlling the resistive switching hysteresis in VO2 thin films via application of pulsed voltage," *Appl. Phys. Lett*, vol. 117, no. 6, pp. 063501, Jul. 2020. doi: 10.1063/5.0017784

[9] J. Q. Lin, S. Ramanathan, and S. Guha, "Electrically driven insulator-metal transition-based devices-part II: transient characteristics," *IEEE T. Electron Dev*., vol. 65, no. 9, pp. 3989-3995, Sep. 2018. doi: 10.1109/TED.2018.2859188.

[10] L. Patlagan et al., "Pulsed vs dc I-V measurements on $Al_xV_{1-x}O_2$ ($x = 0$–0.013) single crystals: Unmasking a non-thermal electric field effect on these crystals," *Appl. Phys. Lett.* vol. 119, no. 22, pp. 221901, Nov. 2021. doi: 10.1063/5.0073797.

[11] R. Naik B., D. Verma, and V. Balakrishnana, "Effect of chemical doping on memristive behavior of VO_2 microcrystals," *Appl. Phys. Lett.* Vol.120, no. 16, pp. 062101, Feb 2022. doi: 10.1063/5.0075566

[12] E. Corti et al., "Scaled resistively-coupled VO_2 oscillators for neuromorphic computing," *Solid State Electron.*, vol. 168, Jun. 2020. doi: 10.1016/j.sse.2019.107729.

[13] E. Corti et al., "Coupled VO_2 oscillators circuit as analog first layer filter in convolutional neural networks," (in English), *Front. Neuronsci.* , Original Research vol. 15, pp. 19, Feb. 2021. doi: 10.3389/fnins.2021.628254.

[14] L. Yann, C Cortes, C. J. C. Burges, "The MNIST database of handwritten digits." http://yann. lecun. com/exdb/mnist/ (1998).

[15] K. Rogers, "An X-ray diffraction study of semiconductor and metallic vanadium dioxide," *Powder Diffr.*, vol. 8, no. 4, pp. 240-244, Dec. 1993. doi: 10.1017/S0885715600019448.

[16] J. Lin et al., "Physics and technology of electronic insulator-to-metal transition (E-IMT) for record high on/off ratio and low voltage in device applications," in *IEDM Tech. Dig.*, San Francisco, CA, USA, Dec. 2017, pp. 23.4.1–23.4.4, doi: 10.1109/IEDM.2017.8268446.

[17] D. Li et al., "Joule Heating-Induced Metal–Insulator Transition in Epitaxial VO_2/TiO_2 Devices," *ACS Appl. Mater. Inter.*, vol. 8, no. 20, pp. 12908-12914, May 2016. doi: 10.1021/acsami.6b03501.

[18] A. Joushaghani et al., "Electronic and thermal effects in the insulator-metal phase transition in VO_2 nano-gap junctions," *Appl. Phys. Lett.*, vol. 105, no. 23, p. 231904, Aug. 2014. doi: 10.1063/1.4903806

[19] T. Hennen et al., "Forming-free Mott-oxide threshold selector nanodevice showing s-type NDR with high endurance (> 10 12 cycles), excellent V th stability (5%), fast (< 10 ns) switching, and promising scaling properties," in *IEDM Tech. Dig.*, San Francisco, CA, USA, Dec. 2018, pp. 37.5.1-37.5.4. doi: 10.1109/IEDM.2018.8614618.

[20] J. M. Goodwill, A. A. Sharma, D. Li, J. A. Bain, and M. Skowronski, "Electro-thermal model of threshold switching in TaO_x-based devices," *ACS Appl. Mater. Inter.,* vol. 9, no. 13, pp. 11704-11710, Mar. 2017. doi: 10.1021/acsami.6b16559.

[21] J. M. Goodwill et al., "Spontaneous current constriction in threshold switching devices," *Nat. Commun.,* vol. 10, no. 1, pp. 1-8, Apr. 2019. doi: 10.1038/s41467-019-09679-9

[22] T. Yajima, T. Nishimura, and A. Toriumi, "Analog spike processing with high scalability and low energy consumption using thermal degree of freedom in phase transition materials," *Proc. IEEE Symp. VLSI Technol.*, Jun. 2018, pp. 27-28. doi: 10.1109/VLSIT.2018.8510649

[23] W. Yi, K. K. Tsang, S. K. Lam, X. Bai, J. A. Crowell, and E. A. Flores, "Biological plausibility and stochasticity in scalable VO2 active memristor neurons," *Nat. Commun.,* vol. 9, no. 1, pp. 1-10, Nov. 2018. doi: 10.1038/s41467-018-07052-w.

[24] S. Cheng et al., "Inherent stochasticity during insulator–metal transition in VO_2," *P. Natl. Acad. Sci.*, vol. 118, no. 37, Sep. 2021. doi: 10.1073/pnas.2105895118.

[25] J. Yoon, G. Lee, C. Park, B. S. Mun, and H. Ju, "Investigation of length-dependent characteristics of the voltage-induced metal insulator transition in VO_2 film devices," *Appl. Phys. Lett.*, vol. 105, no. 8, pp. 083503, May 2014. doi: 10.1063/1.4893783.

[26] J. Lappalainen, S. Heinilehto, H. Jantunen and V. Lantto. "Electrical and optical properties of metal-insulator-transition VO_2 thin films," *J. Electroceram* vol. 22, no.1 pp. 73–77, Feb. 2008. doi: 10.1007/s10832-008-9433-2.

[27] A. Zylbersztejn and N. F. Mott, "Metal-insulator transition in vanadium dioxide," *Phys. Rev. B*, vol. 11, no. 11, pp. 4383-4395, Jun. 1975. doi: 10.1103/PhysRevB.11.4383.

[28] C. Griffiths and H. Eastwood, "Influence of stoichiometry on the metal-semiconductor transition in vanadium dioxide," *J. Appl. Phys*., vol. 45, no. 5, pp. 2201-2206, Jan. 1974. doi: 10.1063/1.1663568.

[29] P. U. Diehl, and M. Cook. "Unsupervised learning of digit recognition using spike-timing-dependent plasticity." *Front. Comput. Neurosci.* vol. 9, 2015, no. 99, Aug. 2015, doi: 10.3389/fncom.2015.00099.

[30] M. Jerry, A. Parihar, B. Grisafe, A. Raychowdhury, and S. Datta,"Ultra-low power probabilistic IMT neurons for stochastic sampling machines," in *Proc. Symp. VLSI Technol.*, vol. 8., Kyoto, Japan, 2017, pp. T186–T187, doi: 10.23919/VLSIT.2017.7998148.

[31] A. Sengupta, P. Panda, P. Wijesinghe, Y. Kim, & K. Roy "Magnetic tunnel junction mimics stochastic cortical spiking neurons," *Sci. Rep.*, vol. 6 no. 1, pp. 1-8, Jul. 2016. doi: 10.1038/srep30039.

[32] H. Hananel et al. "Bindsnet: A machine learning-oriented spiking neural networks library in python," *Front. Neuroinform.* Vol. 12, no. 89, Dec. 2018, doi: 10.3389/fninf.2018.00089.

[33] P. Knag, J. K. Kim, T. Chen, & Z. Zhang. "A sparse coding neural network ASIC with on-chip learning for feature extraction and encoding," *IEEE J. Solid-State Circuits* , Vol. 50 no. 4, pp. 1070-1079, Jan. 2015, doi: 10.1109/JSSC.2014.2386892.